Article

Plasma Dynamics Characterization for Improvement of Resonantly Enhanced Harmonics Generation in Indium and Tin Laser-Produced Plasmas

Vyacheslav V. Kim [1] , **Jelena Butikova** [2] , **Jurgis Grube** [2] , **Anatolijs Sarakovskis** [2] and **Rashid A. Ganeev** [1,3,*]

[1] Laboratory of Nonlinear Optics, University of Latvia, Jelgavas 3, LV-1004 Riga, Latvia
[2] Institute of Solid State Physics, University of Latvia, Kengaraga 8, LV-1063 Riga, Latvia
[3] Tashkent Institute of Irrigation and Agricultural Mechanization Engineers, National Research University, Kori Niyozov Street 39, Tashkent 100000, Uzbekistan
[*] Correspondence: rashid.ganeev@lu.lv

Abstract: In this study, we characterize the properties of indium and tin laser-induced plasmas responsible for efficient high-order harmonics generation of the ultrashort pulses propagating through these media. The optimally formed plasma was determined using the analysis of the time-resolved variations in the spectral and morphological features of spreading indium and tin plasma components under different regimes of laser ablation. We report the measurements of plasma velocities under different regimes of ablation and correlate them with the optimal delay between the heating and probe laser pulses for the generation of harmonics with the highest yield. Electron temperatures and densities are determined using the integrated and time-resolved spectral measurements of plasmas. The resonance-enhanced harmonics are compared with other harmonics from the point of view of the modulation of plasma characteristics. The harmonics of 800 and 1200–2200 nm lasers and their second-harmonic fields were analyzed at optimal conditions of Sn and In plasma formation. The novelty of this work is the implementation of the diagnostics of the dynamics of plasma characteristics for the determination of the optimal plasma formation for harmonics generation. Such an approach allows for the demonstration of the maximal harmonic yield from the studied plasma and the definition of the various resonance-induced harmonic generation conditions.

Keywords: laser-induced ablation; plasma characterization; indium plasma; tin plasma; resonance-induced enhancement of harmonics

1. Introduction

The experimental studies of the optical harmonics generation in the plasmas produced on the surfaces of different materials constitute an important research area of the past decade [1–20]. One of the important parameters influencing high-order harmonics generation (HHG) in laser-induced plasmas (LIP) is the resonance enhancement of a single harmonic in the vicinity of the ionic transitions possessing strong oscillator strength [21–24]. The formation of LIP allows for the analysis of the ionic transitions possessing high oscillator strengths (i.e., high gf values, which are the product of the oscillator strength f of an ionic transition and the statistical weight g of the lower level). To the best of our knowledge, no experiments with gases showing the resonance enhancement of a single harmonic have been reported thus far. The only study showing the partial enhancement of a harmonic in Ar gas is attributed to the influence of Fano resonances [25].

Only a few metals (In, Sn, Mo, Te, Cr) upon ablation demonstrate the effect of resonance enhancement of a single harmonic. Among them, two metals (indium and tin) became attractive subjects for HHG and extreme ultraviolet (XUV) spectroscopic studies [26–29] since they also allow the observation of other enhancement-induced effects, such as quasi-phase-matching of harmonics in the vicinity of strong autoionizing states (AIS) and harmonic

enhancement due to the formation of laser-induced small-sized agglomerates. The determination of the conditions of ablation at which the three above processes can be realized simultaneously is an attractive challenge for further studies of HHG in LIP.

One of the approaches to determine these conditions is related to the optimization of various conditions of target ablation and plasma spreading, such as pulse duration, fluence, pulse repetition rate of heating radiation, determination of the concentration of free electrons and ions at different moments from the beginning of laser ablation, optimal relation between the confocal parameter of converting femtosecond pulses and plasma sizes, presence of the agglomerates of atoms and molecules (clusters, quantum dots, and nanoparticles), etc. The final judgment about the best conditions of LIP for HHG can be derived from the empirical observation of the largest conversion efficiency toward harmonic photons generated during this process. It is obvious that such a complex task can be simplified in the case of specific requirements for the plasma and laser conditions.

Here, we investigate the formation of the optimal conditions for HHG while analyzing the dynamics of indium and tin plasma characteristics, such as the decay of plasma emission in UV range and the modulation of velocity of the plasma spreading at different energies of the heating pulses.

Laser-induced breakdown spectroscopy (LIBS) was used for the spectral characterization of plasma emission. By commonly accepted terminology and definition, LIBS is a type of atomic emission spectroscopy, which uses a highly energetic laser pulse as the excitation source. The laser is focused on the studied sample to form the plasma, which contains the atomized and ionized excited samples. The formation of the plasma only begins when the focused laser achieves a certain threshold for optical breakdown, which generally depends on the environment and the target material.

The analysis of plasma is further carried out for different regimes of HHG using the shorter- and longer-wavelength probe pulses (PP). We determine the plasma characteristics such as velocity and geometry of spreading out from the targets, as well as electron temperature and density, and thus define the correlation between the formation of optimal plasma and the highest harmonic yield from the two studied metals (In and Sn) while comparing with previous reports. Then, the harmonics of the 800 and 1200–2100 nm lasers are analyzed at the optimal conditions of Sn and In plasma formation.

2. Experimental Arrangements

The dynamics of the spectral and spatial characteristics of LIP were analyzed using the time-resolved spectroscopic and plasma spreading measurements at different moments from the beginning of ablation (Figure 1a). The heating pulses (HP, 800 nm, 150 ps, 10 Hz) were obtained by separation of the part of the uncompressed laser pulses prior to the compressor (GC). These pulses were focused on the plane slab targets (T) by a spherical lens (L2). The focal spot diameter of pulse radiation at the target surface was adjusted to 300 μm. The optimal fluence of the heating pulses was ~2 J cm^{-2}. We changed this parameter using the calibrated filters. The delay between the HP and PP in the plasma area was maintained by installation of the optical delay line, allowing the variation of this parameter in the range of 30–100 ns. Two targets (indium and tin metal plates; Sigma-Aldrich) were used for plasma formation.

The shapes of the spreading plasmas produced on the surfaces of indium and tin targets (T) were recorded using the gated intensified CCD camera (iCCD). The delay between HP and image capture was controlled by a trigger signal (TS). The delay was varied between 50 ns and 300 ns with the integration time T_{int} = 5 ns. The time-resolved spectra were registered using the collection optics (CO), spectrometer (SP), and second iCCD camera, together with the images of plasma expansion.
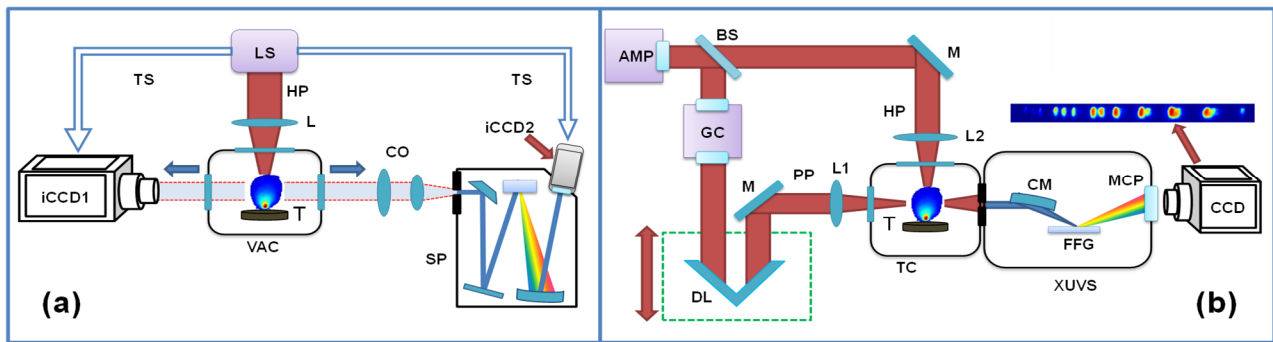
Figure 1. Schematic of the experimental arrangement for (**a**) LIBS and spatial dynamic measurements of plasma and (**b**) HHG. (**a**) LS: laser source, HP: 150 ps heating pulses, L: focusing lens, VAC: vacuum chamber for target (T), TS: trigger signal, SP: spectrometer, iCCD1 and iCCD2: gated intensified CCD cameras for imaging and spectra registration, CO: collection optics. (**b**) AMP: amplifier, BS: beam splitter, GC: grating compressor, M: mirrors, DL: optical delay line, L1 and L2: focusing lenses for uncompressed heating pulses (HP) and probe pulses (PP), TC: target chamber, T: target, XUVS: XUV spectrometer, CM: cylindrical mirror, FFG: flat-field grating, MCP: microchannel plate, CCD: charge-coupled camera.

Two laser sources were used for HHG in the indium and tin plasmas. The first laser (Laser1; Tsunami TSA10, Spectra-Physics) producing the 800 nm, 65 fs, 10 Hz pulses was used for the single-color pump (SCP, 800 nm) of LIP. The pulse duration was measured using the autocorrelator. The second harmonic (400 nm) of this radiation was used for the orthogonally polarized two-color pump (800 nm + 400 nm) of plasma. The laser pulses were focused using the 400 mm focal length spherical lens inside the LIP produced in the vacuum chamber (L1, Figure 1b). The second laser (Laser2: HE-TOPAS Prime, Light Conversion) provided the 70 fs pulses that are tunable in the near infrared (NIR, 1200–2200 nm) spectral range, which were used, alongside the second harmonics of those pulses, for HHG. The intensity of PP in both cases (Laser1 and Laser2) was maintained at ~3 × 10^{14} W cm^{-2}.

In most of the following studies, we used the orthogonally polarized two-color (OTC) pump scheme comprising the NIR pulses and orthogonally polarized second-harmonic radiation as a second field. To add the second field, a 0.5 mm or 0.2 mm thick BBO crystal (type I) was installed inside the vacuum chamber on the path of the focused laser pulse (not shown in Figure 1b). The conversion efficiencies of second harmonic pulses in two cases (Laser1 and Laser2) were 14% and 5%, respectively, for the above-mentioned crystals. The use of a second wave allowed studying the resonant enhancement of harmonics in detail. The harmonics were analyzed using the XUV spectrometer (XUVS, Figure 1b).

3. Characterization of Sn and In Laser-Induced Plasmas

Below, we present the studies of the dynamics of LIBS of the indium and tin plasmas in vacuum conditions. The images of In and Sn expanding plasmas were captured using an iCCD to calculate the expansion velocity of the plasma front. For these purposes, the raw images were recorded at different moments from the beginning of ablation using the same iCCD gate time equal to 5 ns. The results are presented in Figure 2.

Plasma spreading was measured by integrating the intensity profile of the image along the corresponding axis. In the longitudinal direction, the X-axis was used, and in the transverse direction, the Y-axis was used. For each integrated profile, we used the 10% intensity threshold, so the distance was measured as the full width at 10% maximum. Initially, the iCCD images were calibrated by capturing the image of a scaled ruler placed in the target position. For each delay between the heating pulse and the capture of iCCD image, 10 images were obtained at refreshed target points by moving the target holder. Then, the calculated distances were averaged.
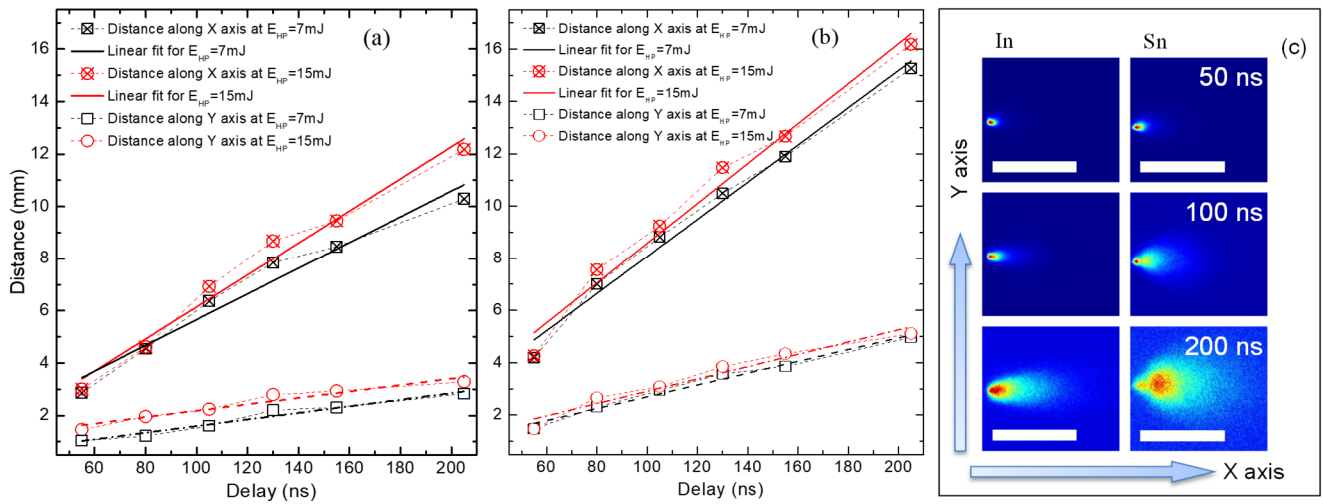
Figure 2. Panels (**a**) (indium LIP) and (**b**) (tin LIP) show the measurements of plasma spreading along the longitudinal X-axis (crossed squares and crossed circles, correspondingly) and along the transverse Y-axis (empty squares and empty circles, correspondingly) at two HP energies (7 mJ, black squares; 15 mJ, red circles). The slopes of the linear fits (black and red solid lines) are used to determine the linear velocity of the emitting front of the plasmas along the X-axis. (**c**) The raw images of plasmas at different delays varying between 50 and 200 ns. White scale bar has length equal to 10 mm.

Both elements (In and Sn) have almost similar atomic weights (114.8 and 118.7, respectively), while the ionization energy is higher for the former atoms (5.78 versus 7.34 eV). The melting temperatures of these metals are relatively low (156.6 and 231.9 °C for In and Sn, respectively). Two HP energies (7 and 15 mJ) were used to study the energy scaling behavior of the plasma spreading. We chose this interval of HP energies given the closeness of these parameters to the optimal fluence of heating pulses for efficient HHG. Table 1 summarizes the calculated velocities of leading fronts of In and Sn plasmas along two axes of spreading. It is obvious that one has to maintain the conditions when the PP propagates through the LIP at the highest concentration of plasma during spreading out from the target surface towards the area of femtosecond pulse propagation. The important parameter strongly influencing harmonic yield from LIP is a delay between HP and PP.

Table 1. Calculated velocities of plasmas along the longitudinal (V_X) and transverse (V_Y) axes using the linear fits of the graphs shown in Figure 2a,b.

	In		Sn	
E_{HP}	V_X ($\times 10^4$ m/s)	V_Y ($\times 10^4$ m/s)	V_X ($\times 10^4$ m/s)	V_Y ($\times 10^4$ m/s)
7 mJ	4.9	1.2	7.1	2.2
15 mJ	6.1	1.2	7.6	2.3

The calculated velocity of spreading plasma allows for estimating the minimum required delay for the leading front of LIP to reach the axis of propagation of the PP focused at a distance of 200 μm from the target's surface. This minimum delay is equal to 5 ns. Meanwhile, the actual optimal delay is larger and corresponds to several tens of nanoseconds. The latter feature is attributed to the heterogeneous distribution of ablated material inside the LIP. Thus, the early time of arrival of the leading front does not correspond to the densest part of plasma.

One can see that the V_x and V_y components of velocities of Sn plasma are sufficiently larger than in the case of In LIP. The velocity of plasma along the X-axis weakly depends on the variation in HP energy. Particularly, the twofold increase in pulse energy (from 7

to 15 mJ) led to an insignificant (~1.3-fold) growth of plasma velocity in the case of In LIP and 1.07× growth in the case of Sn LIP. Meanwhile, the velocity of plasma along the Y-axis remained almost constant for both materials at these two energies of HP.

The time-resolved LIBS measurements were conducted alongside the analysis of LIP spreading (see Figure 1a). Figure 3a,b shows the time-resolved LIBS spectra of In and Sn plasmas measured in the 380–480 nm spectral range for different delays from the beginning of ablation by 15 mJ, 150 ps HP. These spectra demonstrate the groups of In I (410.17 nm, 451.12 nm) and In II (463.8 nm, 465.56 nm, 468.1 nm) lines (Figure 3a), as well as those of Sn I (380.1 nm and 452.47 nm) lines (Figure 3b). One can see a faster decrease in the intensities of emission lines in the case of Sn plasma, which can be associated with the faster removal of ablated material from the area seen by a collection optics (CO, see Figure 1a).
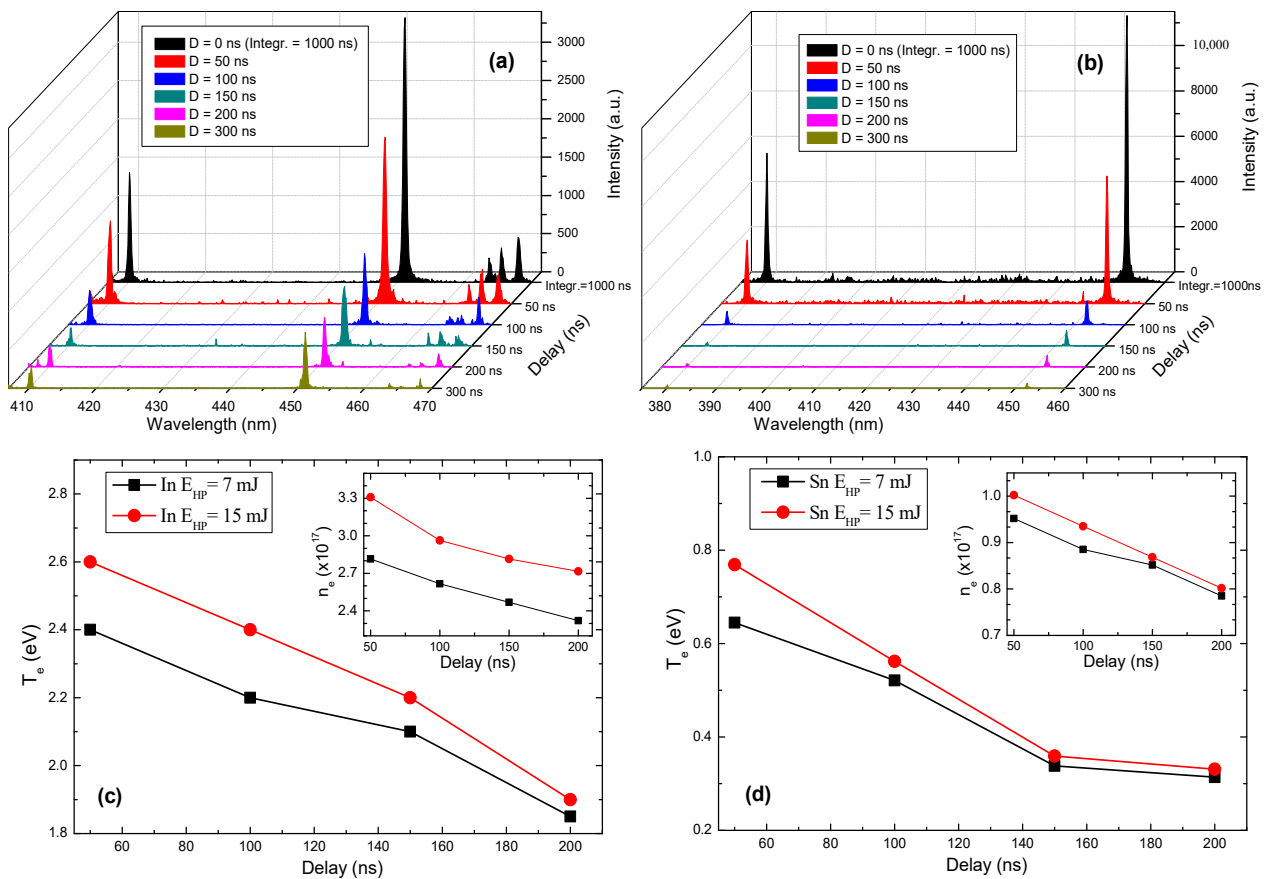

Figure 3. (**a**) The time-resolved spectrum of In plasma in the 400–480 nm range. (**b**) The time-resolved spectrum of Sn plasma in the 390–460 nm range. (**c**,**d**) The results of calculations of the electron temperatures (T_e, in eV) and electron densities (n_e, in cm^{-3}; insets).

Figure 3c,d shows the electron temperatures (T_e) and electron densities (n_e) corresponding to the delays analyzed in Figure 3a,b in the case of two energies (7 and 15 mJ) of HP. The electron temperatures were determined using Boltzmann plots [30], and the electron densities were deduced from Stark broadening of the width of the isolated spectral lines [31,32]. We can note much larger values of electron temperatures and densities in the case of In LIP ($T_e = 2.8$ eV, $n_e = 3.3 \times 10^{17}$ cm^{-3}) compared with Sn LIP ($T_e = 0.8$ eV, $n_e = 1 \times 10^{17}$ cm^{-3}), which can be attributed to the lower ionization energy of indium. This allows us to assume the observation of a stronger resonance (H13, in case of 800 nm pumping) harmonic in the In LIP due to the larger abundance of In$^+$ ions (see the following section).

4. HHG in the Tin and Indium Plasmas at Different Conditions of Ablation

Our studies of HHG in different plasmas produced on the surfaces of chosen targets aimed to determine the correlation between the spatio-spectral measurements of plasma at the specific conditions of laser ablation (i.e., at a variable fluence of 150 ps HP) and the distribution of harmonics along the XUV region while using the PP of variable wavelength and configuration (i.e., SCP and OTC).

4.1. Sn Plasma

Below, we analyze HHG in Sn LIP and demonstrate the correlation between the plasma formation conditions and resonance-induced enhancement of a single harmonic using different laser sources.

The upper image of Figure 4 shows the common feature of the gradually decaying plateau-like harmonic distribution along the whole studied XUV spectrum, except for the single enhanced harmonic (H34) in the case of the 1600 + 800 nm OTC pump. The raw images shown in this figure and others were intentionally taken in the saturation conditions of the CCD camera for better viewing of the peculiarities of harmonic distribution. The presentation of experimental data as the images appearing on the computer screen rather than the groups of intensity distributions was aimed at a better view of the obtained data and a clear demonstration of the difference between the HHG in the cases of the featureless distribution of harmonics (i.e., at the conditions of the gradual decay of harmonic intensity along the whole plateau range) and the resonance-affected distribution of harmonics. We want to stress that the goal of such presentations was the qualitative definition of the conditions when the resonance processes play a decisive role in the enhancement of a single harmonic. This can be clearly seen in the cases of different pumps of the studied plasmas (single-color pulp and two-color pump). Notably, all line-outs of the harmonic spectra shown in the following figures were taken using the images collected in the unsaturated conditions of registration. The difference in the acquisition times in the case of saturated and unsaturated collections of harmonic spectra was 10:2. In other words, in the former case, the CCD camera collected the harmonic spectra over ten shots of laser pulses, while in the latter case, it collected the harmonic spectra with two shots.
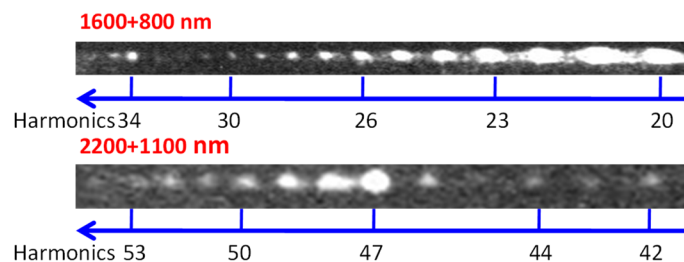

Figure 4. Raw images of harmonic spectra generated in tin plasma in the case of application of Laser2. Upper panel: OTC (1600 + 800 nm) of LIP when H34 was notably stronger than the adjacent harmonics. Bottom panel: OTC (2200 + 1100 nm) of LIP when H47 dominated over other harmonics.

The bottom image of Figure 4 presents the group of harmonics from tin plasma in the range of 46–53 nm using the 2200 + 1100 nm OTC pump. One can see a decayed group of H42–H45 harmonics followed by significantly stronger H47–H49 orders, with further decay up to the cut-off (H53). Notice the closeness of the strongest enhanced harmonic (H47, λ = 46.8 nm) and the resonance transition of Sn II (λ = 47.2 nm).

The comparative spectra of harmonics using 800 nm (Laser1) and NIR (Laser2) pulses are shown in Figure 5. The advantage of studies on the resonance-induced enhancement of harmonics using the tunable optical parametric amplifiers is the opportunity to fine-tune this high-order nonlinear optical process for the enhancement of single harmonic yield. Particularly, the tuning of NIR pulses towards 1310 nm allowed observation of the enhanced 28th harmonic (H28, λ = 46.78 nm) of the two-color pump (1310 + 655 nm) and

two adjacent harmonics (Figure 5, bottom panel). This harmonic was close to the strong ionic transition of tin (47.2 nm). The same transition was responsible for the growth of a single harmonic (H17) in the case of the 800 nm pump (Figure 5, upper panel).
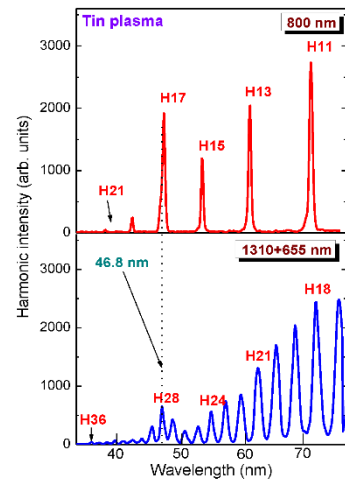

Figure 5. Spectral distribution of harmonics in 33–77 nm spectral range in the case of different pumps of Sn LIP. Upper panel: SCP (800 nm) using Laser1 when H17 (λ = 46.76 nm) was enhanced in the vicinity of strong ionic transition. Bottom panel: OTC (1310 + 655 nm) using Laser2 when H28 was stronger than the adjacent harmonics.

4.2. In Plasma

The raw image of the spectrum of indium plasma is shown in the top panel of Figure 6. One can see the emission in the vicinity of the strong transition (λ = 62.2 nm). The strongest enhancement of a single harmonic among two studied LIPs (Sn and In) was observed in the case of indium plasma and optimal ablation of the target. H13 of 800 nm SCP using Laser1 was significantly stronger than other harmonics (Figure 6, second panel). The analysis of relative intensities showed that H13 was ~70 times higher than adjacent orders.
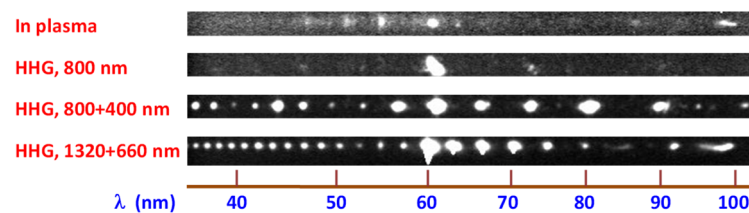

Figure 6. Raw images of plasma and harmonic spectra from the indium ablation. Upper panel: Plasma emission in the case of the over-excitation of In target. Second panel: HHG spectrum using SCP (800 nm, Laser1) at optimal ablation of target. Third panel: HHG spectrum using OTC (800 + 400 nm, Laser1). Fourth panel: HHG spectrum using OTC (1320 + 660 nm, Laser2).

The optimization of plasma formation was aimed at the enhancement of the single harmonic compared with the adjacent ones. The difference between the wavelengths of H11, H13, and H15 was large enough, so the ionic transition affected only one harmonic order (H13) and did not influence the other two adjacent harmonics.

In our experiments, two orthogonally polarized pulses (800 and 400 nm) were overlapped both temporally and spatially in the plasma, which led to a significant enhancement of all odd and even harmonics. OTC drastically modified the harmonic spectrum (third panel of Figure 6). The extension of harmonic cut-off, a significant growth of the yield of odd harmonics compared with that of an SCP (see second panel), and the comparable harmonic intensities for the odd and even orders along the whole range of generation allowed for achieving efficient HHG. Meanwhile, the resonance-induced single harmonic

was not enhanced as strongly as other harmonics during these two-color experiments. In the bottom panel of Figure 6, we also present the results of our studies of the resonance-enhanced single harmonic generation using the NIR pulses and their second harmonic (1320 + 660 nm, Laser2). In this case, the yield of the resonance-enhanced harmonic (H21, λ = 62.85 nm) was also higher than that of other harmonics, though its ratio was not larger than 5 to 10 depending on the harmonic order. We noticed a strong enhancement of the nearby longer-wavelength harmonics (H18–H20).

Another situation occurs when the wavelength difference between the harmonics becomes smaller. For this, we used the 2100 nm idler pulses of Laser2, allowing the generation of the odd harmonics in the vicinity of strong ionic resonance of indium LIP using a 1.7 J cm^{-2} fluence of HP (Figure 7a). We also found that the application of SCP leads to a significant deviation from the featureless homogeneous harmonic distribution. H33 was stronger than any of the lower-order ones. The nearby longer-wavelength harmonic (H31) was almost suppressed, while the nearby shorter-wavelength harmonic (H35) was almost similar to H23–H27. Notice that at weaker ablation (i.e., at a fluence of heating pulse of F = 1.1 J cm^{-2}), the enhancement ratio of H33 and other harmonics was even stronger compared with the above-described case (F = 1.7 J cm^{-2}). This observation illustrates the importance of the optimization of LIP formation for efficient HHG.

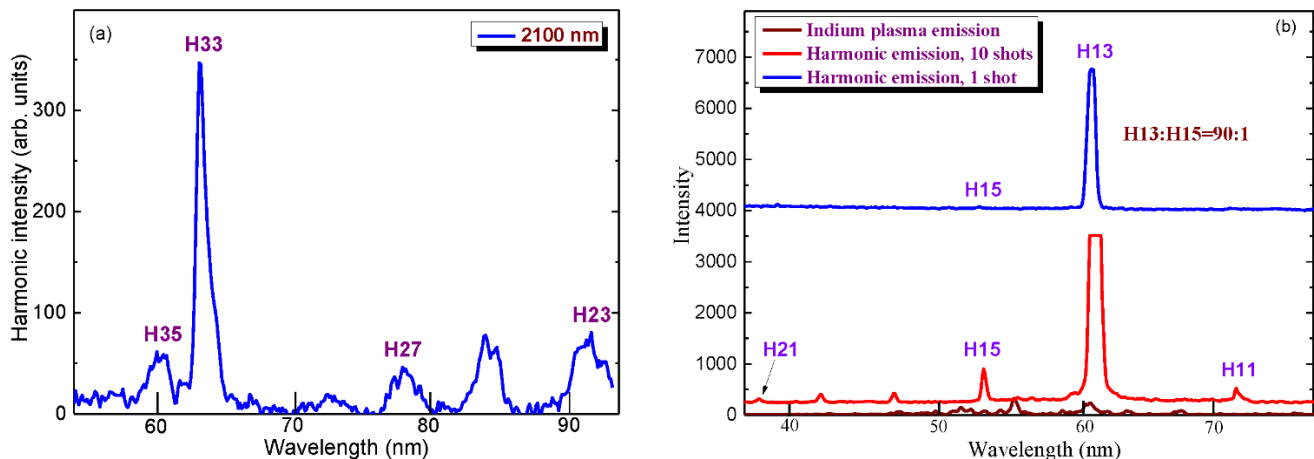**Figure 7.** (**a**) Harmonic distribution from In LIP in the 55–95 nm spectral range in the case of 2100 nm PP (Laser2). (**b**) Determination of the enhancement factor of H13 in the case of 800 nm SCP (Laser1). Two upper curves show the same spectrum retrieved at different collection times to demonstrate the saturated H13 emission (middle curve) and unsaturated H13 emission using a different number of laser shots (10 and 1, respectively). Bottom curve shows the plasma emission spectrum of the over-excited indium LIP.

The quantitative measurements of the enhancement factor of a resonance-enhanced single harmonic were carried out using the SCP (800 nm, Laser1). The harmonic spectra were collected over 1 and 10 laser shots (Figure 7b, two upper curves). In the latter case, H13 demonstrated a notable saturation, which did not allow calculating the ratio of this enhanced harmonic and the nearby strongest harmonic (H15). The collection of HHG spectrum in the case of a single shot (upper curve) led to the determination of this parameter (~90). This enhancement factor depends on various experimental conditions (wavelength of PP, pulse duration, delay between HP and PP, distance from the target surface at which PP propagates through the plasma, plasma formation conditions, etc.). The latter parameter seems crucial for achieving the largest enhancement of a single harmonic. We optimized it by choosing the proper fluence of HP, as well as the optimal delay between HP and PP. These parameters allow for optimizing the velocity of plasma, its temperature, the concentration of plasma and free electrons, the emission of incoherent radiation, etc. We observed that stronger ablation of the target led to the growth of free electron concentration,

which notably decreased the conversion efficiency towards the harmonics due to the phase mismatch. The bottom curve of Figure 7b shows the plasma emission spectrum of the over-excited indium LIP in the conditions of stronger ablation.

One of restricting factors influencing the enhancement of harmonics in the plateau range is a self-phase modulation of PP. To avoid the influence of this process, one must determine the conditions of plasma at which the fundamental radiation does not modify during propagation through the plasma. With smaller plasma width, the influence of self-phase modulation of PP on the enhancement factor of a single harmonic becomes less significant. The same can be said about the influence of the characteristics of PP on HHG in various LIPs. We observed this dependence in the case of manganese plasma, which was used as a medium for HHG, and compared it with indium LIP (Figure 8, two bottom raw images of harmonic spectra in the case of Laser1). The increase in the intensity of fundamental radiation (from $I_1 = 3 \times 10^{14}$ W cm^{-2} to $I_2 = 6 \times 10^{14}$ W cm^{-2}) led to the broadening and blue-shift of harmonics, alongside the increase in HHG conversion efficiency. One can see that the higher-order harmonics (for example, H15–H29) in the case of In plasma (upper panel of Figure 8) remain stronger than those from Mn plasma even at a lower intensity of the fundamental radiation in the former case. The three images were collected in similar experimental conditions.
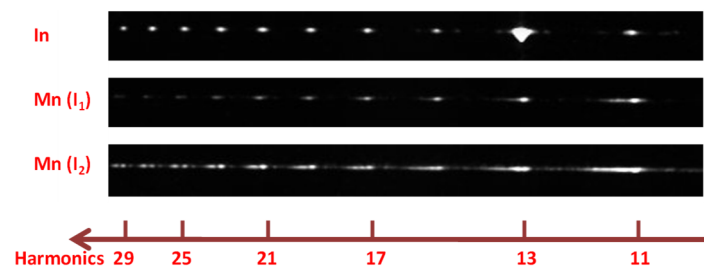

Figure 8. Raw images of harmonic spectra from 800 nm pump (Laser1) in the case of In (upper panel) and Mn (two bottom panels) LIPs. The harmonic spectra in the case of Mn plasma were obtained at two different intensities of PP ($I_1 = 3 \times 10^{14}$ W cm^{-2} and $I_2 = 6 \times 10^{14}$ W cm^{-2}).

The harmonics generated in indium plasma using NIR pulses (Laser2) were expectedly weaker compared with the case of the 800 nm pump (Laser1) due to the λ^{-5} wavelength-dependent yield of harmonics. The comparison of these two pumps of tin LIP at similar energies of pulses (1 mJ) showed an anticipated decrease in the harmonic yield in the plateau region using 1310 nm pulses compared with the 800 nm pulses (Figure 5). We also used the weak idler pulses from the optical parametric amplifier ($\lambda = 2100$ nm) with the energy varying in the range of 0.3 to 0.5 mJ for harmonic generation in plasma. Even these small energies of longer-wavelength PP were sufficient to observe the resonance enhancement of some harmonic orders near the AIS of indium (Figure 7a).

5. Discussion

The novelty of this work is the implementation of the diagnostics of LIP characteristics for the determination of the "optimal plasma" formation for HHG. The term "optimal plasma" refers to conditions when the process of harmonics generation can be carried out in the most efficient mode. This means that the plasma allows (a) the demonstration of the maximal harmonic yield from the studied LIPs and (b) the demonstration of the resonance-induced harmonic generation for the specific harmonic order.

Previous HHG studies in LIPs were mostly empirical observations of this process in different plasmas. Of course, in early studies, the characteristics of plasma were also taken into account. However, there was little attention to quantitatively measure the dynamics of plasma and match them with the demands for efficient HHG. Most of those studies were carried out using the analysis of the integrated characteristics of plasma. Meanwhile, the modification of plasma at each moment of excitation and spreading out from target was

not taken into account. We believe that the present study is the first one combining the characterization of variable plasma and matching its characteristics with the requirements for the maximal harmonic yield during propagation of the femtosecond pulses through such plasma.

The general task in these experiments was to determine the velocity of the movement of the plasma front, as well as to calculate the temperature and density of free electrons in LIP. Below, we address the question of why the delay time between the acquisition system and the ablated sample is important for the determination of the variable characteristics of LIP. The images of the extending plasma plume inside the vacuum chamber from the surface of indium and tin targets were recorded using the gated intensified CCD camera. As was mentioned, the delay varied between 50 ns and 300 ns. We captured the plasma emission spectra and plasma spreading at the interval between 50 and 55 ns, then 55 and 60 ns, etc. This allowed us to determine the decay of plasma emission spectrum over almost the whole period of plasma excitation, spreading out from the target, and the decay of emission alongside the broadening of plasma volume. The earlier moments of plasma formation (i.e., between 0 and 50 ns delay) are not important for the determination of the process of optimal plasma formation for HHG at the used intensities of heating pulses. The images of In and Sn expanding plasmas were also obtained using an iCCD to estimate the expansion velocity of the plasma plumes.

The resonance-related effects play an important role in different fields of laser physics and optics. Studies of this process during HHG of ultrafast laser pulses in Sn plasma have appeared in a few publications [27,33,34]. Those studies were mostly focused on the difference in the resonance-enhanced high-order harmonic generation in atomic and nanoparticle laser-induced tin plasmas, the application of the OTC pump of tin plasma, and other peculiarities of this process. Meanwhile, various properties such as dynamics of plasma spreading, spectral variations in incoherent emission, and other aspects were not studied.

The resonance enhancement of a single harmonic (H17 of 795 nm laser, $\lambda = 46.76$ nm) has previously been observed and attributed to the influence of some ionic transitions of tin possessing strong oscillator strength [33]. Previously, Sn II ion was shown to possess a strong transition $4d^{10}5s^25p^2P_{3/2}$–$4d^95s^25p^2(^1D)^2D_{5/2}$ at the wavelength of 47.20 nm [35]. The *gf* value of this transition has been calculated to be 1.52. This value is five times larger than other transitions from the ground state of Sn II. Therefore, the enhancement of H34 ($\lambda = 47.06$ nm) using the 1600 nm + 800 nm pump in the case of Laser2 (upper panel of Figure 4) can be explained as being due to the optimal closeness to the above-mentioned transition.

The enhancement of the H13 of 800 nm PP (Laser1), H22 of 1320 nm pump (Laser2), and H33 of 2100 nm pump (Laser2) in the case of indium plasma is due to the influence of the radiative transitions between the $4d^{10}5s^2$ $^1S_0$ ground state of In II and the low-lying $4d^95s^2np$ transition array of In II. Among them, the AIS of In II at 19.92 eV ($\lambda = 62.24$ nm, $4d^{10}5s^2$ $^1S_0$–$4d^9$ $5s^2$ $5p^1$ P_1) is exceptionally strong. The oscillator strength of this transition has been calculated to be *gf* = 1.11 [36], which is more than 12 times larger than that of any other transitions of In II. This transition is energetically close to the above-mentioned harmonics of different sources of pump radiation, thereby resonantly enhancing their intensity. Moreover, as one can see, this transition affects the harmonic yield of some adjacent harmonic orders as well, which is manifested by higher yields of those harmonics compared with the lower-order ones. The first observation of this process in the indium plasma was reported in [26] using SCP.

Application of the OTC laser field is frequently reported in studies of HHG in gases and laser-induced plasmas. This field commonly consists of two linearly polarized laser pulses with frequencies ω and 2ω and mutually orthogonal polarizations. Particularly, HHG in the case of the homonuclear diatomic molecules exposed to an OTC was reported in [37]. The authors analyzed the harmonic ellipticity as a function of the ratio of the intensities of the OTC laser field components and their relative phase. The emission rate and ellipticity

of high-order harmonics generated exposing a homonuclear diatomic molecule, aligned in the laser-field polarization plane, to a strong OTC laser field was also studied in [38]. In the case of HHG in LIP, the OTC approach led to a significant improvement of the conversion efficiency, harmonic cutoff, and similar intensities of the odd and even harmonics [39–43]. Various advantages in that case were emphasized while demonstrating better conditions for quasi-phase matching of generating harmonics, resonance enhancement of even orders, application in nanomaterials, etc.

In our experiments, the conversion efficiency of second harmonic pulses was low due to the position of the thin BBO placed on the path of the *focused* laser beam, i.e., in conditions when the converting beam possessed large divergence. Commonly, the notably larger conversion of the fundamental beam to the second harmonic can be achieved during the application of the beam possessing small divergence, while using the propagation of the plane wave through the crystal, contrary to our case; otherwise, the phase-matching conditions for second-harmonic generation will be disrupted. In our case, we did not insert the nonlinear crystal in front of the focusing lens, since the propagation of two beams (800 and 400 nm) through the lens and window of the vacuum chamber causes a significant delay between these two pulses. This delay does not allow efficient interaction of 800 and 400 nm pulses inside the LIP and correspondingly restricts the advantages of OTC during HHG. We did not use the Michelson-like scheme to combine two pulses (800 and 400 nm) in the plasma area. We also did not apply the calcite inside the vacuum chamber to create the conditions when these two pulses perfectly overlap in the time domain. Our OTC scheme is extremely simple—we either installed our crystal inside the vacuum chamber on the path of the focused radiation or removed it to work in the regime of OTC pump or SCP.

Additionally, we used the thin BBO crystals to allow the overlap of two pulses (fundamental and second harmonic) in the plasma area. The group velocity dispersion significantly increases a delay of the fundamental beam with regard to the second harmonic in this negative crystal. Thus, one must use as thin as possible crystals to diminish this impeding factor.

The used small conversion efficiency of second-harmonic radiation was sufficient for demonstration of the influence of an extremely weak orthogonal second wave on the overall pattern of HHG spectrum, which is one of the advantages of these studies in the case of optimized LIP. Moreover, we were able to demonstrate the odd and even harmonics generation at rather smaller ratios of the energies of orthogonally polarized second-harmonic and fundamental beams (1:50, i.e., at 2% conversion efficiency). Correspondingly, the increase in second-harmonic conversion efficiency is not a necessary requirement for the improvement of the studied process of HHG using OTC pump configuration. The greater intensity of the second harmonic can cause some negative consequences, such as stronger yield of even harmonics compared with odd ones due to the $I_h \infty \lambda^{-5}$ rule depicting the influence of the wavelength of converting radiation on the harmonic yield.

6. Conclusions

We have shown that apart from the difference in the consistency of harmonic emitters (i.e., atoms or ions), proper excitation of the ablated targets is crucial in the formation of the conditions where the resonance-induced processes start playing important roles in the modification of the harmonic distribution, from a featureless, gradually decaying pattern of harmonics to a spectrum containing strong harmonics in the shorter-wavelength range. We demonstrated the method of laser-induced plasma formation and characterization for efficient HHG during ablation of indium and tin and propagation of femtosecond pulses through the optimally adjusted plasmas. The dynamics of studied plasma spreading out from the target surface were correlated with the maximal harmonic yield for the non-resonant harmonics and resonance-enhanced harmonic. Plasma velocities under different regimes of ablation were analyzed from the point of view of determination of the optimal delay between the heating pulses used for target ablation and converting femtosecond probe pulses propagating through the studied plasmas. Laser-induced breakdown spectroscopy

was used for the optimization of the fluencies of the heating pulses and determination of electron temperature and density. The enhancement factors of resonance-induced harmonics have shown a direct relation with the optimization of plasma characteristics.

In general, the novelty of this work is the implementation of the diagnostics of plasma characteristics for the determination of the "optimal plasma" formation for HHG. The term "optimal plasma" refers to conditions when the process of harmonics generation can be carried out in the most suitable manner. It means that this plasma allows (a) the demonstration of the maximal harmonic yield from the studied LIPs and (b) the demonstration of resonance-induced harmonic generation conditions for the specific harmonic order.

Author Contributions: Conceptualization, R.A.G.; Formal analysis, R.A.G., V.V.K. and A.S.; Investigation, V.V.K., J.B., J.G. and A.S.; Methodology, R.A.G.; Supervision, R.A.G.; Visualization, V.V.K.; Writing—Original draft, R.A.G.; Writing—Review and editing, R.A.G., V.V.K., J.B., J.G. and A.S. All authors have read and agreed to the published version of the manuscript.

Institutional Review Board Statement: Not applicable.

Informed Consent Statement: Not applicable.

Data Availability Statement: The data that support the findings of this study are available from the corresponding author upon reasonable request.

Conflicts of Interest: The authors declare no conflict of interest.

References

1. Elouga-Bom, L.B.; Bouzid, F.; Vidal, F.; Kieffer, J.-C.; Ozaki, T. Correlation of plasma ion densities and phase matching with the intensities of strong single high-order harmonics. *J. Phys. B* **2008**, *41*, 215401. [CrossRef]
2. Singhal, H.; Arora, V.; Rao, B.S.; Naik, P.A.; Chakravarty, U.; Khan, R.A.; Gupta, P.D. Dependence of high-order harmonic intensity on the length of preformed plasma plumes. *Phys. Rev. A* **2009**, *79*, 023807. [CrossRef]
3. Pertot, Y.; Elouga-Bom, L.B.; Bhardwaj, V.R.; Ozaki, T. Pencil lead plasma for generating multimicrojoule high-order harmonics with a broad spectrum. *Appl. Phys. Lett.* **2011**, *98*, 101104. [CrossRef]
4. Elouga-Bom, L.B.; Pertot, Y.; Bhardwaj, V.R.; Ozaki, T. Multi-µJ coherent extreme ultraviolet source generated from carbon using the plasma harmonic method. *Opt. Express* **2011**, *19*, 3077–3085. [PubMed]
5. Elouga-Bom, L.B.; Haessler, S.; Gobert, O.; Perdrix, M.; Lepetit, F.; Hergott, J.-F.; Carré, B.; Ozaki, T.; Salières, P. Attosecond emission from chromium plasma. *Opt. Express* **2011**, *19*, 3677–3683. [CrossRef]
6. Haessler, S.; Bom, L.B.E.; Gobert, O.; Hergott, J.-F.; Lepetit, F.; Perdrix, M.; Carré, B.; Ozaki, T.; Salières, P. Femtosecond envelope of the high-harmonic emission from ablation plasmas. *J. Phys. B* **2012**, *45*, 074012. [CrossRef]
7. Pertot, Y.; Chen, S.; Khan, S.D.; Elouga-Bom, L.B.; Ozaki, T.; Chang, Z. Generation of continuum high-order harmonics from carbon plasma using double optical gating. *J. Phys. B* **2012**, *45*, 074017. [CrossRef]
8. Kumar, M.; Singhal, H.; Chakera, J.A.; Naik, P.A.; Khan, R.A.; Gupt, P.D. Study of the spatial coherence of high order harmonic radiation generated from preformed plasma plumes. *J. Appl. Phys.* **2013**, *114*, 033112. [CrossRef]
9. Haessler, S.; Strelkov, V.; Elouga-Bom, L.B.; Khokhlova, M.; Gobert, O.; Hergott, J.-F.; Lepetit, F.; Perdrix, M.; Ozaki, T.; Salieres, P. Phase distortions of attosecond pulses produced by resonance-enhanced high harmonic generation. *New J. Phys.* **2013**, *15*, 013051. [CrossRef]
10. Singhal, H.; Naik, P.A.; Kumar, M.; Chakera, J.A.; Gupta, P.D. Enhanced coherent extreme ultraviolet emission through high order harmonic generation from plasma plumes containing nanoparticles. *J. Appl. Phys.* **2014**, *115*, 033104. [CrossRef]
11. Rosenthal, N.; Marcus, G. Discriminating between the role of phase matching and that of the single-atom response in resonance plasma-plume high-order harmonic generation. *Phys. Rev. Lett.* **2015**, *115*, 133901. [CrossRef] [PubMed]
12. Fareed, M.A.; Thire, N.; Mondal, S.; Schmidt, B.E.; Legare, F.; Ozaki, T. Efficient generation of sub-100 eV high-order harmonics from carbon molecules using infrared laser pulses. *Appl. Phys. Lett.* **2016**, *108*, 124104. [CrossRef]
13. Fareed, M.A.; Strelkov, V.V.; Thire, N.; Mondal, S.; Schmidt, B.E.; Legare, F.; Ozaki, T. High-order harmonic generation from the dressed autoionizing states. *Nat. Commun.* **2017**, *8*, 16061. [CrossRef] [PubMed]
14. Wostmann, M.; Splitthoff, L.; Zacharias, H. Control of quasi-phase-matching of high-harmonics in a spatially structured plasma. *Opt. Express* **2018**, *26*, 14524. [CrossRef] [PubMed]

15. Fareed, M.A.; Strelkov, V.V.; Singh, M.; Thire, N.; Mondal, S.; Schmidt, B.E.; Legare, F.; Ozaki, T. Harmonic generation from neutral manganese atoms in the vicinity of the giant autoionization resonance. *Phys. Rev. Lett.* **2018**, *121*, 023201. [CrossRef]
16. Kumar, M.; Singhal, H.; Chakera, J.A. High order harmonic radiation source for multicolor extreme ultraviolet radiography of carbon plumes. *J. Appl. Phys.* **2019**, *125*, 155902. [CrossRef]
17. Singh, M.; Fareed, M.A.; Laramée, A.; Isgandarov, E.; Ozaki, T. Intense vortex high-order harmonics generated from laser-ablated plume. *Appl. Phys. Lett.* **2019**, *115*, 231105. [CrossRef]
18. Liang, J.; Lai, Y.H.; Fu, W.; Shan, Y.; Yu, W.; Guo, C. Observation of resonance-enhanced high-order harmonics from direct excitation of metal nanoparticles with femtosecond pulses. *Phys. Rev. A* **2020**, *102*, 053117. [CrossRef]
19. Konda, S.R.; Soma, V.R.; Banavoth, M.; Ketavath, R.; Mottamchetty, V.; Lai, Y.H.; Li, W. High harmonic generation from laser-induced plasmas of Ni-doped CsPbBr3 nanocrystals: Implications for extreme ultraviolet light Sources. *ACS Appl. Nano Mater.* **2021**, *4*, 8292–8301. [CrossRef]
20. Konda, S.R.; Lai, Y.H.; Li, W. Investigation of high harmonic generation from laser ablated plumes of silver. *J. Appl. Phys.* **2021**, *130*, 013101. [CrossRef]
21. Milošević, D.B. High-energy stimulated emission from plasma ablation pumped by resonant high-order harmonic generation. *J. Phys. B At. Mol. Opt. Phys.* **2007**, *40*, 3367. [CrossRef]
22. Strelkov, V. Role of autoionizing state in resonant high-order harmonic generation and attosecond pulse production. *Phys. Rev. Lett.* **2010**, *104*, 123901. [CrossRef]
23. Milošević, D.B. Resonant high-order harmonic generation from plasma ablation: Laser intensity dependence of the harmonic intensity and phase. *Phys. Rev. A* **2010**, *81*, 023802. [CrossRef]
24. Tudorovskaya, M.; Lein, M. High-order harmonic generation in the presence of a resonance. *Phys. Rev. A* **2011**, *84*, 013430. [CrossRef]
25. Rothhardt, J.; Hadrich, S.; Demmler, S.; Krebs, M.; Fritzsche, S.; Limpert, J.; Tunnermann, A. Enhancing the macroscopic yield of narrow-band high-order harmonic generation by Fano resonances. *Phys. Rev. Lett.* **2014**, *112*, 233002. [CrossRef]
26. Ganeev, R.A.; Suzuki, M.; Baba, M.; Kuroda, H.; Ozaki, T. Strong resonance enhancement of a single harmonic generated in extreme ultraviolet range. *Opt. Lett.* **2006**, *31*, 1699–1701. [CrossRef]
27. Ganeev, R.A.; Strelkov, V.V.; Hutchison, C.; Zaïr, A.; Kilbane, D.; Khokhlova, M.A.; Marangos, J.P. Experimental and theoretical studies of two-color pump resonance-induced enhancement of odd and even harmonics from a tin plasma. *Phys. Rev. A* **2012**, *85*, 023832. [CrossRef]
28. Ganeev, R.A.; Wang, Z.; Lan, P.; Lu, P.; Suzuki, M.; Kuroda, H. Indium plasma in the single- and two-color mid-infrared fields: Enhancement of tunable harmonics. *Phys. Rev. A* **2016**, *93*, 043848. [CrossRef]
29. Abdelrahman, Z.; Khohlova, M.A.; Walke, D.J.; Witting, T.; Zair, A.; Strelkov, V.V.; Marangos, J.P.; Tisch, J.W.G. Chirp-control of resonant high-order harmonic generation in indium ablation plumes driven by intense few-cycle laser pulses. *Opt. Express* **2018**, *26*, 15745–15758. [CrossRef]
30. Balki, O.; Rahman, M.M.; Elsayed-Ali, H.E. Optical emission spectroscopy of carbon laser plasma ion source. *Opt. Commun.* **2018**, *412*, 134–140. [CrossRef]
31. Burger, M.; Skočić, M.; Ljubisavljević, M.; Nikolić, Z.; Djeniže, S. Spectroscopic study of the laser-induced indium plasma. *Eur. Phys. J. D* **2014**, *68*, 223. [CrossRef]
32. Konjević, N.; Lesage, A.; Fuhr, J.R.; Wiese, W.L. Experimental Stark widths and shifts for spectral lines of neutral and ionized atoms (A critical review of selected data for the period 1989 through 2000). *J. Phys. Chem. Ref. Data* **2002**, *31*, 819. [CrossRef]
33. Suzuki, M.; Baba, M.; Ganeev, R.; Kuroda, H.; Ozaki, T. Anomalous enhancement of single high-order harmonic using laser ablation tin plume at 47 nm. *Opt. Lett.* **2006**, *31*, 3306. [CrossRef]
34. Ganeev, R.A.; Kuroda, H. Reexamining different factors of the resonance-enhanced high-order harmonic generation in atomic and nanoparticle laser-induced tin plasmas. *Appl. Sci.* **2021**, *11*, 2193. [CrossRef]
35. Duffy, G.; van Kampen, P.; Dunne, P. 4d→5p transitions in the extreme ultraviolet photoabsorption spectra of Sn II and Sn III. *J. Phys. B* **2001**, *34*, 3171. [CrossRef]
36. Duffy, G.; Dunne, P. The photoabsorption spectrum of an indium laser produced plasma. *J. Phys. B* **2001**, *34*, L173. [CrossRef]
37. Habibović, D.; Gazibegović-Busuladžić, A.; Busuladžić, M.; Čerkić, A.; Milošević, D.B. Laser-induced processes with homonuclear diatomic molecules in orthogonally polarized two-color laser field. *J. Phys. Conf. Ser.* **2021**, *1814*, 012001. [CrossRef]
38. Habibović, D.; Milošević, D.B. Ellipticity of high-order harmonics generated by aligned homonuclear diatomic molecules exposed to an orthogonal two-color laser field. *Photonics* **2020**, *7*, 110. [CrossRef]
39. Suzuki, M.; Ganeev, R.A.; Ozaki, T.; Baba, M.; Kuroda, H. Enhancement of two-color high harmonic by using two compound strong radiative transition ions in double-target scheme. *Appl. Phys. Lett.* **2007**, *90*, 261104. [CrossRef]
40. Ganeev, R.A.; Singhal, H.; Naik, P.A.; Kulagin, I.A.; Redkin, P.V.; Chakera, J.A.; Tayyab, M.; Khan, R.A.; Gupta, P.D. Enhancement of high-order harmonic generation using two-color pump in plasma plumes. *Phys. Rev. A* **2009**, *80*, 033845. [CrossRef]
41. Ganeev, R.A.; Hutchison, C.; Zaïr, A.; Witting, T.; Frank, F.; Okell, W.A.; Tisch, J.W.G.; Marangos, J.P. Enhancement of high harmonics from plasmas using two-color pump and chirp variation of 1 kHz Ti:sapphire laser pulses. *Opt. Express* **2012**, *20*, 90–100. [CrossRef]

42. Ganeev, R.A.; Boltaev, G.S.; Kim, V.V.; Venkatesh, M.; Zvyagin, A.I.; Smirnov, M.S.; Ovchinnikov, O.V.; Wöstmann, M.; Zacharias, H.; Guo, C. High-order harmonic generation using quasi-phase matching and two-color pump of the plasmas containing molecular and alloyed metal sulfide quantum dots. *J. Appl. Phys.* **2019**, *126*, 193103. [CrossRef]

43. Konda, S.R.; Soma, V.R.; Ganeev, R.A.; Banavoth, M.; Ketavath, R.; Li, W. Third-order optical nonlinearities and high-order harmonics generation in Ni-doped CsPbBr$_3$ nanocrystals using single- and two-color chirped pulses. *J. Mater. Sci.* **2022**, *57*, 3468–3485. [CrossRef]